Proceedings of the ASME 2020 15th International Manufacturing Science and Engineering Conference
MSEC2020
September 3, 2020, Virtual, Online

MSEC2020-8461

SIMULATION AND CHARACTERIZATION OF COLD SPRAY DEPOSITION OF METAL POWDERS ON POLYMER SUBSTRATE ELECTRICALLY CONDUCTIVE APPLICATION

Jung-Ting Tsai, David F. Bahr
School of Materials Engineering, Purdue University
West Lafayette, IN

Semih Akin, Fengfeng Zhou,
Martin Byung-Guk Jun[1]
School of Mechanical Engineering, Purdue University
West Lafayette, IN

MinSoo Park
Seoul National University of Science and Technology
Department of Mechanical System Design Engineering
Seoul, South Korea

ABSTRACT

Cold sprayed polymer substrates offer a promising platform for bridging electroless deposition methods and applications. This study's contribution to the field is the combination of cold sprayed polymer substrate and the electroless-plating process. In simulation, finite element analysis of the as-sprayed polymer substrate using a viscoelastic model that considers large strain time-dependent behavior were conducted. A three-network constitutive model was applied to capture the non-linear and time-dependent response of large strain polymer deformation. In experiment, the process-structure-property relationship was examined from the as-sprayed specimen to the final coated electroless-plated samples. A controlled coating process of Cu powders was first cold sprayed on polyamide 6. The as-sprayed specimen was then electroless deposited. Mechanical testing was performed on as-sprayed specimens and adhesion testing was performed on electroless deposited specimens. Scanning electron microscopy (SEM) was employed to observe the surface and the cross-section of the as-sprayed and electroless deposited specimens. Lastly, the behavior of Cu coated specimens immersed in KOH solution was examined by cyclic voltammetry.

Keywords: Cold spray, polyamide 6, finite element analysis, conductive pattern and electroless copper plating

1. INTRODUCTION

Cold spray deposition has been used in maintenance repair operation (MRO) and additive manufacturing (AM) for metal to metal bonding for decades[1-3]. Depending on the input pressure capability of the cold spray system, the output pressure allows the particles to reach supersonic speed and be plastically deformed onto the substrate material. The heavily plastic deformed particle traps the heat within the interface (adiabatic shear instability) of the particle and the substrate. This ultimately allows the temperature at the interface to increase and therefore instead of strain-hardening of the material, the interface strain-softens [4, 5]. Recent studies have examined cold spraying polymer substrates, often to increase the electrical conductivity of the polymer substrate. The cold sprayed particles do not necessarily need to be pre-heated. This method benefits from using a Cu powder coating without oxidation of the particles. Unlike other methods such as screen-printing or inkjet-printing, the cold spray system is non-solvent based and provides a wide range of particle morphology and sizing. The technique provides easy maneuverability of the sprayed pattern, an accessible large area of coating, and no temperature requirement for spraying. These advantages are beneficial for industrial efficiency and provides an affordable, robust, and less relatively rapid method for coating applications [6-10].

Cold spray metal on polymer has been extensively studied. The common issues that cold spray faces are the difficulties of accumulating a uniform thickness of the conductive layer on the polymer substrate and often only a single particle successfully impinged into the polymer substrate. With continuous particles impacting the substrate, the particles erode the original interlock particles within the polymer substrate. This not only wastes the powders but destroys the already coated surface [6, 7, 9-11]. While some articles have addressed a process window for a successful coating layer, it remains challenging because of the lack of understanding between the connection of the coating

[1] Contact author: mbgjun@purdue.edu

process (cold spraying) and the material structure (as-sprayed substrate). To understand the basic phenomenon between particle and substrate, researchers have performed a simulation model attempting to describe the deposition process. Mostly the simulation models only considered metal (particle) impacting metal (substrate). The simulation results demonstrated that particle/substrate morphology changes with increasing velocity and addressed how the kinetic energy initiate the bonding between the interface. Continued studies are still being conducted, which assist in understanding metal to metal coating but limit the understanding of metal to polymer coating. In which case, the polymer substrate is sensitive to impact forces, strain rate, and temperature. All the factors influence the outcome performances of coated polymer substrate.

Generally, cold spraying metal on polymer shows good adhesion strength compared with other coating methods. Thus, it is proposed to use an electroless deposition method to coat polymer specimens after being cold sprayed. This is to achieve an electrically coating pattern on the polymer substrate and avoiding a long duration of cold spray that causes the surface to be damaged. Therefore, in the essence of what has already been done towards the current gap, this paper plans to first look into the structural-property relationship of an as-sprayed specimen and bridging the method of using electroless deposition after cold spraying the substrate. This is because, in the electroless community, they often encounter the difficulty of coating on a non-conductive substrate or a flexible design pattern on a substrate [12, 13]. The bridging between a cold sprayed specimen towards the electroless deposition process solved the current dilemma. A designed cold sprayed pattern can move on to the electroless deposition and coating with a conductive pattern.

2. MATERIALS AND METHODS

2.1 Cold spray setup

FIGURE 1 shows a schematic of a typical design of a CS apparatus. Compressed air (1-4 MPa) first flows through the system. The channel of flow merges with the path of the powder feeder. The spray nozzle is designed with a converging/diverging de Laval-type. This permits the gas and the particle to reach supersonic speed on the exit from the nozzle towards the surface.

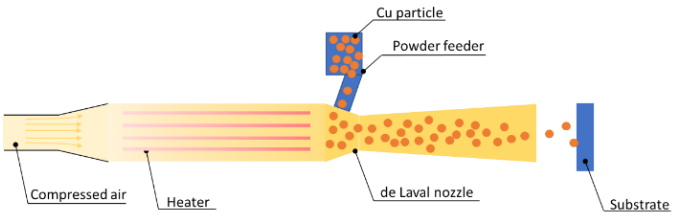

FIGURE 1 SCHEMATIC OF COLD SPRAY PROCESS

2.2 Material properties

Often the CS feedstock used gas-atomized powder to avoid clogging of the spray nozzle. The CS process is effective by using solid powders (1-100 μm in diameter) flowing through the channel and sprayed out through a designed nozzle at the supersonic speed. In this study, copper particle (Sigma-Aldrich Co., USA) and polyamide (ePlastic Co., USA) were used. The particle morphology of the Cu powders is shown in FIGURE 2. The particle size is roughly spherical and distributed in the range of 1-10 μ m. The microstructures of the as-sprayed and electroless-deposited specimens was also examined. The surface and the cross-section area were observed using scanning electronic microscopy (SEM, JEOL-6500F) (shown in **FIGURE 2**).

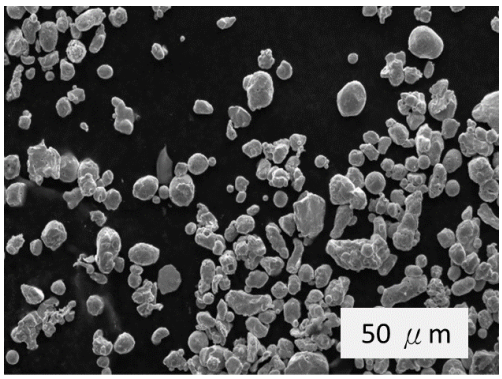

FIGURE 2 CU PARTICLE MORPHOLOGY

2.3 Test methods and apparatus

A 22 KIP hydraulic MTS 810 load frame was used in this experiment for the tensile test and the adhesion test. The crosshead displacement rate was 1 mm/min according to the ASTM D3039 [14]. According to ASTM C633 [15], the adhesive strength of the substrate/coating interface is measured by adhesively attaching the substrate/coating specimen to the caps (fixtures) and then applying a tensile force onto the fixtures, as shown in FIGURE 3 to cause the substrate/coating dis-bonding. The substrate/coating can display a cohesive fracture with crack propagating through the coating layer or an adhesive fracture at the substrate-coating interface. The test results are disregarded if the substrate/coating disbands from the caps. The adhesion strength of the coating on polymer substrate (<20 MPa) is typically much lower than the adhesive strength of the specimen/fixture bond (250 MPa) [10].

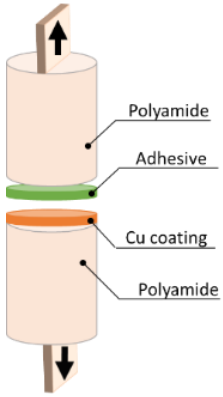

FIGURE 3 ADHESION TEST SETUP SCHEMATIC

The volume resistivity (electrical resistivity) was measured by a four-probe apparatus (FIGURE 4(a)). The four-probe was designed with the outer two probes measuring current and the inner two probes measuring voltage (FIGURE 4(b)). Several coated distances were measured to determine the volume resistivity per-cross-sectional area by utilizing the following equation (1):

$$R = \rho \frac{\ell}{A} \quad (1)$$

Where R is the electrical resistance of the coat layer on the substrate calculated from the measured current and voltage; ρ is the electrical volume resistivity; ℓ is the length of the specimen; A is the cross-section area of the coated layer.

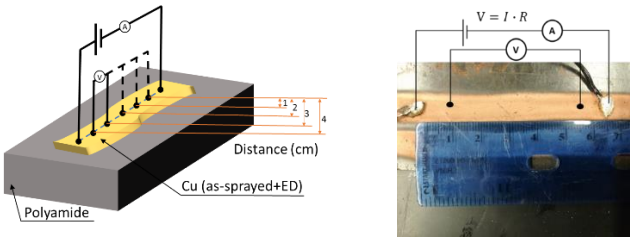

(a) A SCHEMATIC OF SETUP (b) EXPERIMENTAL MEASUREMENT

FIGURE 4 FOUR-POINT PROBE MEASUREMENT PROCESS

Lastly, the electrochemical measurement was performed on a SP-300 Biologics equipped with the Elab software. All the as-sprayed and electroless deposition specimens were cleaned with DI water so the surface is not attached to residual chemicals. The voltammetry cycle for E was set from 3.5 to -4 (V); scan rate 80 mV/s. This setup is typical for electrochemical experiments which have a 3 electrodes system, the commercial reference (Ag/AgCl), the counter electrode and the working electrode. The working electrode in this test is the specimen.

2.4 Electroless-plating material and process

After cold sprayed, the specimens were immersed in the electroless-plating solution for 2 hr, 4 hr, 8 hr, 16 hr, and 24 hr. The Cu electroless bath solution followed the industrial standard. The solution formula is organized in Table 1 and the general chemical reaction is shown in equation (2). The Cu sulfate is a soluble salt that allows reducing of the oxide deposited on the as-sprayed surface. The EDTA and the Hydrochloric acid is a complex agent that improves the quality of the deposition. The sodium hydroxide acts as a buffer that controls the pH and to obtain an equivalent amount of thin and uniform plating. The Potassium ferricyanide assists the plating rate. Finally, the formaldehyde solution is a reducing agent that initiates the metal ions deposition process. The deposition rate control, the deposition thickness, and the connection with the chemical solution can be found in the work of Mishra and Paramguru [13], [16]. This research will be focusing on the connection between sprayed specimens towards the electroless plating process.

$$Cu_2+ + H_2PO_2 + H2O \rightarrow Cu + H_2PO^{3-} + 2H^+ \quad (2)$$

Table 1 CU ELECTROLESS DEPOSTION FORMULA

Content	Volume (g/mole)
Cu sulfate	100~200
EDTA	250-300
Sodium hydroxide	40-45
Hydrochloric acid	35-45
Pottassium ferricyanide	400-500
DI water	1 liter
Formaldehyde solution	30-40

3. SIMULATION MODELING AND ANALYSIS

3.1 Simulation properties

To simplify the simulation, it is assumed a perfectly spherical Cu particle with a diameter of 40 μm impacting a polymer substrate. Also, the particle only considered a vertical impact with no rotation. The particle impacting polyamide 6 was simulated using the commercially available finite element analysis software ABAQUS/EXPLICIT 2018 equipped with PolyUMod ®. A two-dimensional axisymmetric model was presented. The bottom of the substrate is fixed, and a symmetry boundary condition of the X-plane is fixed along the Y-axis. The ALE numerical method was used in this research. This approach combines with the Lagrangian analysis and Eulerian analysis to mitigates the heavily distorted element nodes from the impact. The re-defined nodes accelerated the calculation process. The substrate is assumed to be ten times the particle radius (20 μm). This is to avoid the reflecting waves traveling back to the impact area and causing unnecessary deformation. The general contact friction coefficient at the interface was set at 0.3 for each study. To obtain an accurate simulation, the particle and the substrate used a 0.02 μm mesh size. A 4-node bilinear plain strain quadrilateral element was used for both the particle and the substrate.

3.2 Material model

The elastic region of the material was assumed to be linear for Cu and polyamide 6. The thermal response is not considered in this study but will be in future research. Material properties are shown in Table 2. The Johnson-Cook plasticity model is assigned to the Cu particle which is the expression (3):

$$\sigma = [A + B\varepsilon^n][1 + C \ln \dot{\varepsilon}^*][1 - T^{*m}] \quad (3)$$

where A is yield stress, B is hardening constant, C is strain rate constant, n is hardening exponent, m is thermal softening exponent, and T is temperature variation

Table 2 MATERIAL CONSTANTS USED IN THE JOHNSON-COOK PLASTICITY MODEL (CU PARTICLE)

Material property	Material constants

ρ(kg/m3)	8.9 x 10^3
G (GPa)	44.7
A (MPa)	90
B (MPa)	292
n	0.31
C (MPa)	0.025
m	1.09
Tm (K)	1356
To (K)	298

The polyamide 6 substrate was simulated using an already developed three network model which consists of three parts (molecular networks) acting in parallel [17]. The three parallel network model will be stated as A, B, and C. More details and validation of this model can be find in XXX. This model was specifically developed for thermoplastic materials which are the expression shown in
(4),
(5), and
(6):

$$\sigma_A = \frac{\mu_A}{J_A^e \bar{\lambda}_A^{e^*}} * \frac{\mathcal{L}^{-1}(\frac{\bar{\lambda}_A^{e^*}}{\lambda_L})}{\mathcal{L}^{-1}(\frac{1}{\lambda_L})} * dev[b_A^{e^*}] + \kappa(J_A^e - 1)I \quad (4)$$

$$\sigma_B = \frac{\mu_B}{J_B^e \bar{\lambda}_B^{e^*}} * \frac{\mathcal{L}^{-1}(\frac{\bar{\lambda}_B^{e^*}}{\lambda_L})}{\mathcal{L}^{-1}(\frac{1}{\lambda_L})} * dev[b_B^{e^*}] + \kappa(J_B^e - 1)I \quad (5)$$

$$\sigma_C = \frac{\mu_C}{J\ \lambda_{chain}} * \frac{\mathcal{L}^{-1}(\frac{\lambda_{chain}}{\lambda_L})}{\mathcal{L}^{-1}(\frac{1}{\lambda_L})} * dev[b^{e^*}] + \kappa(J - 1)I \quad (6)$$

where $J_A^e = det[F_A^e]$, $b_A^{e^*} = J_A^{e^{-2/3}} F_A^e (F_A^e)^T$, $\bar{\lambda}_A^{e^*} = (tr[b_A^{e^*}/3])^{1/2})$, $\mathcal{L}(x) = coth(x) - \frac{1}{x}\mu$, A is the shear modulus of network A, λ_L is the locking stretch, τ_A is flow resistance of network A, mA and mB is the stress exponential of network A and B, μ_{Bi} and μ_{Bf} is the initial and final shear modulus of network B, β is the evolution rate, and τ_B is the flow resistance of network

The total results of the Cauchy stress in this system is given by the sum of the stresses in the three-network model. The material constants for the material model are listed in Table 3. The material constant numbers were taken from the experimental results of a Split Hopkinson pressure bar tested on a polymer substrate [18].

Table 3 MATERIAL CONSTANTS USED IN THE THREE-NETWORK MODEL (POLYAMIDE 6 SUBSTRATE)

Material property	Material constants
μ_A (MPa)	2350.68
λ_L(MPa)	7.52
Kappa	3500
τ_A (MPa)	13
m_A	7.63
μ_{Bi} (MPa)	547.26
μ_{Bf} (MPa)	154.32
β	12.08
τ_B (MPa)	65.75
m_B	15.71
muC	1.62

3.3 Impact morphology

The simulation results shown in FIGURE 5 (a-c) reveal the Cu particle impact into the polymer substrate's morphology. The particle initial velocity speed is set as 50 m/s, 150 m/s, and 300 m/s and the particle size diameter is set as 40 μm for all three testing conditions. The particle size is set for 40 μm to explore to common case of input simulation particle diameter (the maximum size is 60 μm for typical. This simulation value of the particle initial velocity is set between 50 m/s – 300 m/s was due to the cold spray system input air pressure is set between 80 psi to 100 psi. The correlation between the pressure and the initial velocity is been validate and used by Che, Chu, Vo and Yue [7]. The compression ratio was taken from the original Cu shape and after impacting. The maximum value of rebound velocity is taken from the Cu particle after impacting the polymer substrate and separating from it. The rebound kinetic energy value was taken from the rebound velocity and a set mass value. Unlike metal particles impacting a metal substrate that spits metal at the interface, the simulation results show the particle impinges into the polyamide 6 substrate without any spits of the polymer. The results show that as the initial velocity increases, the Cu particle impinges into the polymer substrate substantially. In FIGURE 5 (d), the three impact velocities are plotted against the compression ratio of the Cu particle after the rebound of the particle. At 50 m/s (shown in FIGURE 5 (e), after impact the particle retained its original shape and the rebound velocity was lower compared to the impact velocity if 150 m/s and 300 m/s . The compression ratio of the Cu particle increases while the polymer substrate was heavily deformed as the impact velocity increases. In FIGURE 5 (e), the rebound velocity and the rebound kinetic energy are plotted with impact velocity. The results show with increasing impact velocity, the rebound velocity, and the rebound kinetic energy increase proportionally. The analytical deformation data obtained from the simulation results can be used for future analysis of the copper particles.

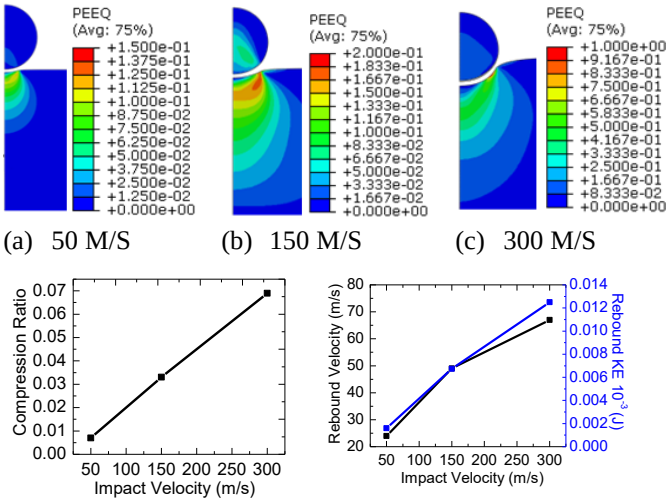

(a) 50 M/S (b) 150 M/S (c) 300 M/S

(d) CU COMPRESSION RATIO AFTER REBOUND (e) REBOUND VELOCITY AND KINETIC ENERGY AT INCREASING IMPACT VELOCITY

FIGURE 5 SIMULATION RESULTS OF A CU PARTICLE (40 UM) IMPACTING POLYAMIDE 6 AT THREE DIFFERENT IMPACT VELOCITIES.

In FIGURE 6 (a-c), the impact velocity was set as 300 m/s and the particle size was adjust from 5 μm, 10 μm, and 40 μm. For metal to metal bonding, the impact velocity is typically around 600 m/s (Cu particle to Cu substrate). The hardness of polymers is smaller than metal and therefore it is assumed that the Cu particle can impinge into a polymer substrate at half of the impact velocity which is 300 m/s. In FIGURE 6 (d), the Cu particle compression ratio increases as the particle size decreases. This explains that a smaller particle is more likely to deformed than bigger particle size at constant impact velocity. In FIGURE 6 (e), the rebound kinetic energy increases while the rebound velocity decrease with increasing particle size. This explains that a smaller particle has less rebound kinetic energy and is therefore likely to stick onto the polymer substrate. On the other hand, a larger particle is likely to have a higher kinetic energy and be less inclined to attach onto the polymer substrate.

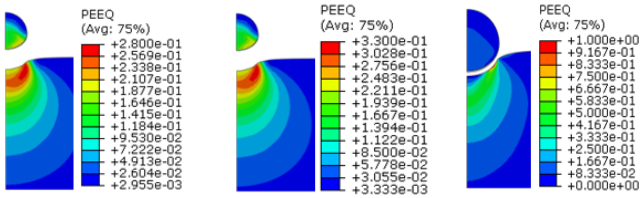

(a) 5 UM (b) 10 UM (c) 40 UM

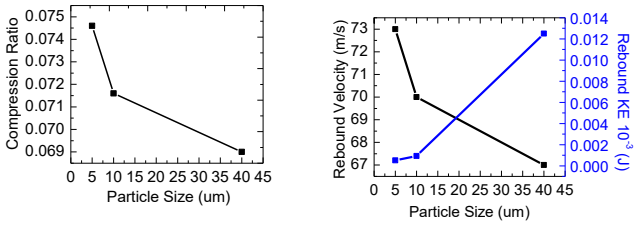

(d) CU COMPRESSION RATIO AFTER REBOUND (e) REBOUND VELOCITY AND KINETIC ENERGY AT INCREASING PARTICLE SIZE

FIGURE 6 SIMULATION RESULTS OF THREE OF DIFFERENT CU PARTICLE SIZES IMPACTING POLYAMIDE AT 300 M/S

4. EXPERIMENTAL RESULTS AND DISCUSSION

4.1 As-sprayed specimen mechanical strength

The tensile test was carried out to see if the cold spray process causes structural damage to the polymer substrate. The polyamide 6 dog bone specimen was manufactured in which the thickness of the specimen is 0.2 mm [14].The polyamide 6 dog-bone specimens which are label as PA1 and PA2 are the unsprayed specimens while the PA1+CS and PA2+CS are the sprayed specimens. The tensile strength was compared with the sprayed and the unsprayed specimens. For the sprayed specimens, a one pass was done to conduct the coating. However, some of the region is not coated with Cu powders. This was made intentionally to observe if the un-coated area may have any overall influence towards the tensile strength. As the results indicate, the coated specimens still retained their tensile strength compared with the uncoated coupon (FIGURE 7). No significant increase or deterioration of tensile strength was observed within the sprayed specimens.

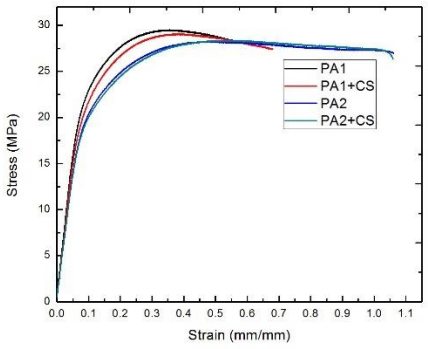

FIGURE 7 TENSILE TEST RESULTS OF AS-SPRAYED SPECIMENS

4.2 Microstructure of as-sprayed and after electroless-plating specimens

In FIGURE 8, the top surface of the as-sprayed specimen after, 2 hours, 4 hours, 8 hours, 16 hours, and 24 hours of electroless deposition are displayed. The as-sprayed specimen

shows the single-particle attached firmly onto the polymer substrate. As times increase, the electroless solution starts to form Cu layers on the as-sprayed specimens. The particles fill the gap between the cold sprayed particle with increasing growth of the size. At 24 hours deposition, the surface was covered with Cu particles and no porosity between particles can be seen compared with the as-sprayed specimen.

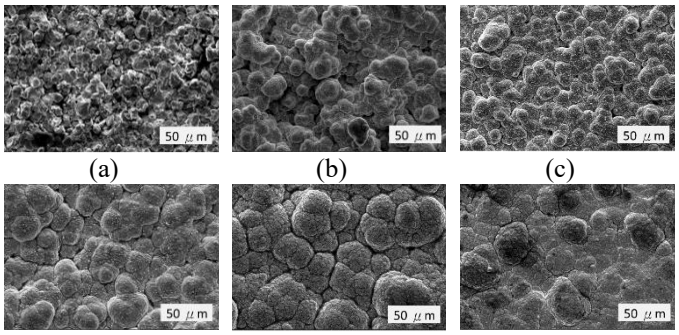

FIGURE 8 TOP SURFACE OF (A) AS-SPRAYED SPECIMENS AND ELECTROLESS-DEPOSITION OF (B)2 HR, (C) 4 HR, (D) 8 HR (E) 16 HR ,AND (F) 24 HR

In **FIGURE 9**, the cross-section of the as-sprayed specimen, 2 hours, 4 hours, 8 hours, 16 hours, and 24 hours of electroless deposition are shown. The cross-section of as-sprayed specimens shows the splat morphology, voids, defects, and interface boundaries between the particle-particle and particle-substrate junctions. As the electrical deposition time increases, the deposition thickness increases. At 24 hours deposition, the average thickness reaches 50 μm. The cold sprayed particles have formed into a bulk conductive layer with the electroless deposition of Cu.

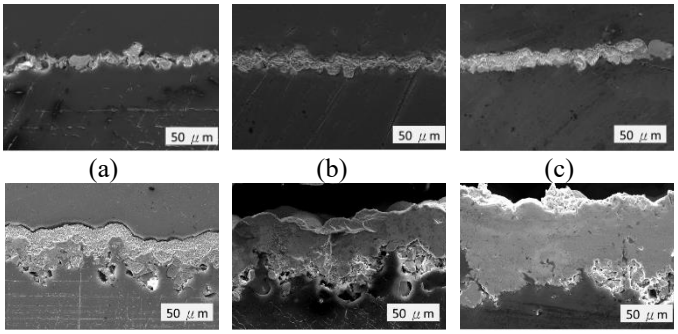

FIGURE 9 CROSS-SECTION OF (A) AS-SPRAYED SPECIMENS AND ELECTROLESS-DEPOSITION OF (B)2 HR, (C) 4 HR, (D) 8 HR (E) 16 HR ,AND (F) 24 HR

4.3 Adhesion test results

Adhesion testing was conducted on as-sprayed specimens, electroless deposition of 4 hr specimens, and 16 hr specimens. Each of the testing conditions has three specimens. After testing, each set of test results were averaged (shown in TABLE 4. The adhesion strength of as-sprayed specimens is the highest amount for the electroless coating conditions. The adhesion strength decreases as the electroless deposition time increases. While the adhesion test suggested that the specimens should have a flat surface between the connections of the coated surface, it is difficult to fully achieve in this test. It can be observed that the as-sprayed specimens and the electroless-deposited specimens have high roughness and surface contour (shown in FIGURE 8 and FIGURE 9). This may overall influence the results of the adhesion strength. For all the as-sprayed specimens, the failure occurs between the epoxy and the polyamide 6 sides. The same failing occurs in the 4 hr specimens. However, for the 16 hr specimens, an adhesion failure occurs between the metal and the epoxy (half of the coated Cu metal attached on the epoxy while the other half are on the polyamide side). While this testing follows the ASTM C633 [15] and provides a qualitative results but the quantitative results are not promising.

TABLE 4 ADHESION TEST OF AS-SPAYED AND ELECTROLESS DEPOSITION SPECIMENS

NO	Adhesion strength (MPa)	Electroless (hr)
1	10.2 (STD 0.35)	0
2	7.5 (STD 0.81)	4
3	4.8 (STD 1.15)	16

4.4 Electrical property

The theoretical electrical resistivity value of bulk copper is around 2.65×10^{-8} (Ω-m). The four-point probe method was measured on all the coated specimen. The concept is to prove that the Cu coated layer is conductive. The measured value of electrical resistivity ranges from 5.3×10^{-6} (Ω-m) to 2.16×10^{-7} (Ω-m) (Specimens from 4 hr- 24 hr). The measured value was one magnitude value worse than the bulk copper. We suspect this is because the surface roughness, voids and defects caused by improper electroless plating condition play a significant role in the measurement. An on-going investigation is still conducted to improve a higher conductivity from cold sprayed specimens and the electroless deposition method.

4.5 Voltammetry test results

The behavior of Cu and CuO in 0.4 M KOH was examined by cyclic voltammetry. The 24 hr of electroless deposition specimen were used to conduct a cyclic voltammetry test. The coated specimen is the working electrode in this experiment. In FIGURE 10, the x-axis is the applied potential E while the y-axis is the response of the current. The reduction and oxidation curve were cycled for five times to see the stability. The scan rate is set as a constant. The results demonstrate a potential tool to probe reactions between electron transfers and further research in sensor application.

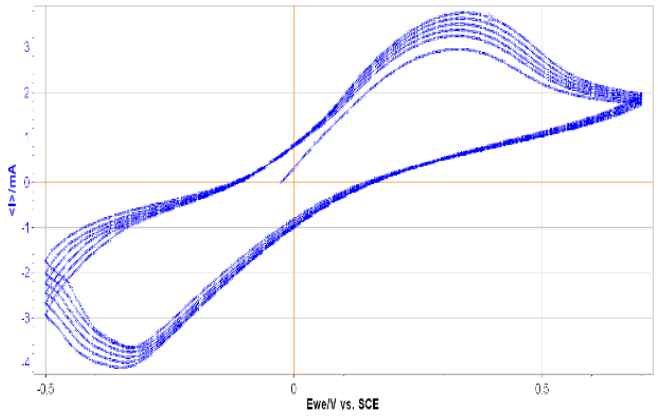

FIGURE 10 CYCLIC VOLTAMMETRY TEST OF 24 HR ELECTROLESS-DEPOSITION SPECIMEN

5. CONCLUSION

The as-sprayed substrate provides a promising platform for a multi-functional manufacturing application. In this study, a polyimide 6 substrate was deposited with continuous Cu particles with various times of electroless deposition. Finite element analysis was conducted to simulate the morphology changes of Cu particle impacting on a polymer substrate. A viscoelastic model was implemented to the substrate to capture the copper impact. The result shows that the impacted of the polymer substrate is differently from metal to metal impact. A constant particle size with an increasing impact velocity was simulated. The results show that with an increasing impact velocity, the particle deformation increases. Also, the rebound velocity and the kinetic energy increases. However, at constant impact velocity with decreasing particle size, small particles tend to be more deformable than bigger particles. The kinetic energy decreases while the rebound velocity increase with increasing particle size. The as-sprayed specimens still retained their tensile strength after cold sprayed. The surface and the cross-section of the as-sprayed and Cu electroless deposited specimens were examined. The adhesion test was conducted, and the results show that adhesion strength decrease as the coating layer increases. The final coated specimens were examined with a cyclic voltammetry test to demonstrate the feasibility of an electrochemical application tool.

ACKNOWLEDGEMENTS

The author acknowledges Xingyu Fu and Ziyuan Cheng for preparing the samples in this work. Also, the author thanks Purdue EPICS program for facilitating the cold spray system and Jorge Martinez for providing the space for accommodating the cold spray machine.

REFERENCES

[1] S. Yin, X. Wang, X. Suo, H. Liao, Z. Guo, W. Li, C. Coddet, Deposition behavior of thermally softened copper particles in cold spraying, Acta Materialia 61(14) (2013) 5105-5118.
[2] T. Schmidt, H. Assadi, F. Gärtner, H. Richter, T. Stoltenhoff, H. Kreye, T. Klassen, From Particle Acceleration to Impact and Bonding in Cold Spraying, Journal of Thermal Spray Technology 18(5) (2009) 794.
[3] B. Samareh, A. Dolatabadi, A Three-Dimensional Analysis of the Cold Spray Process: The Effects of Substrate Location and Shape, Journal of Thermal Spray Technology 16(5) (2007) 634-642.
[4] G. Bae, Y. Xiong, S. Kumar, K. Kang, C. Lee, General aspects of interface bonding in kinetic sprayed coatings, Acta Materialia 56(17) (2008) 4858-4868.
[5] T. Schmidt, F. Gärtner, H. Assadi, H. Kreye, Development of a generalized parameter window for cold spray deposition, Acta Materialia 54(3) (2006) 729-742.
[6] Z. Khalkhali, W. Xie, V.K. Champagne, J.-H. Lee, J.P. Rothstein, A comparison of cold spray technique to single particle micro-ballistic impacts for the deposition of polymer particles on polymer substrates, Surface and Coatings Technology 351 (2018) 99-107.
[7] H. Che, X. Chu, P. Vo, S. Yue, Metallization of Various Polymers by Cold Spray, Journal of Thermal Spray Technology 27(1) (2018) 169-178.
[8] P. Cavaliere, Cold-Spray Coatings - Recent Trends and Future perspectives, Springer International Publishing, 2018.
[9] S. Shah, J. Lee, J.P. Rothstein, Numerical Simulations of the High-Velocity Impact of a Single Polymer Particle During Cold-Spray Deposition, Journal of Thermal Spray Technology 26(5) (2017) 970-984.
[10] A. Małachowska, M. Winnicki, Ł. Konat, T. Piwowarczyk, L. Pawłowski, A. Ambroziak, M. Stachowicz, Possibility of spraying of copper coatings on polyamide 6 with low pressure cold spray method, Surface and Coatings Technology 318 (2017) 82-89.
[11] S. Deng, L. Djukic, R. Paton, L. Ye, Thermoplastic–epoxy interactions and their potential applications in joining composite structures – A review, Composites Part A: Applied Science and Manufacturing 68 (2015) 121-132.
[12] T. Anik, M. Touhami, K. Himm, S. Schireen, R. Belkhmima, M. Abouchane, M. Cissé, Influence of pH Solution on Electroless Copper Plating Using Sodium Hypophosphite as Reducing Agent, International Journal of Electrochemical Science 7 (2012).
[13] K.G. Mishra, R. Paramguru, Surface modification with copper by electroless deposition technique: An overview, African Journal of Pure and Applied Chemistry 4 (2010) 87-99.
[14] Standard Test Method for Tensile Properties of Polymer Matrix Composite Materials.
[15] Standard Test Method for Adhesion or Cohesion Strength of Thermal Spray Coatings, 2017.
[16] S.S. Djokić, Fundamentals of Electroless Deposition, 2016.
[17] J. Bergström, A. Bowden, C. Rimnac, S. Kurtz, Development and Implementation of an Advanced User Material Model for UHMWPE, (2019).
[18] H. POURIAYEVALI, Describing Large Deformation of Polymers at Quasi-static and High Strain Rates, 2013.